

Piston compression of semiflexible ring polymers in channels

Peter Cifra and Tomáš Bleha*

Polymer Institute, Slovak Academy of Sciences, 84541 Bratislava, Slovakia

E-mail: cifra@savba.sk

Keywords: wormlike chains, simulations, compression elasticity, nanochannels, confinement regimes, double-folded hairpins, shrinking factor

We use molecular simulations in nanochannels to explore the compression elasticity of ring polymers of stiffness (persistence length) similar to DNA. By combination with the parallel data for linear polymers, we assess the effect of chain topology on their compression behavior. The results show that the ring polymers are much less bendable at longitudinal compression than the linear analogs. The chain span of linear polymers is continuously reduced at compression, whereas in ring polymers an abrupt decrease of the span is observed. The simulation data elucidate this phenomenon as the buckling of a ring polymer into the double-folded hairpin. The shrinking ratio of sizes of the ring and linear chains shows a complex behavior much differing from the existing reports. The force-displacement functions for chains of both topologies at moderate confinement are very well accounted for by the mean-field Flory scheme. The theory predicts the difference in the mechanical stiffness of the ring and linear polymers in qualitative agreement with the simulation data. These findings are relevant to the compression behavior of semiflexible ring polymers under spatial constraints such as in nanofluidic experiments, disordered media, or cellular environment.

1. Introduction

The field of man-made cyclic polymers has in the last decades rapidly advanced on the synthetic, characterization, and applications fronts^[1, 2]. The naturally occurring ring polymers are best epitomized by circular DNA found in most bacteria as a bacterial chromosome, and as plasmids in the cytoplasm. The cyclic (ring) polymers exhibit different physical and biological properties in comparison with the linear counterparts. Constraining a polymer into a ring topology has a profound impact on chain conformations and dynamics. Because of the absence of end groups, the ring chains are more compact than the linear ones, and the reptation mechanism of their movement is entirely suppressed. The conformation properties of ring polymers are affected by the chain rigidity. The stiffness of ring chains encompasses a broad range, from the highly flexible chains such as poly(ethylene oxide) up to rather stiff helical chains such as circular DNA and cyclic amylose derivatives^[3].

The biological functions and technological applications of ring polymers often involve operation under spatial constraints such as the crowded cellular milieu or the porous matrix. The impact of the geometric confinement on properties of polymers is well understood in molecules of linear topology^[4, 5]; the analogous impact on the ring analogs is less explored^[6-12]. Current insights into the behavior of confined polymers much rest on the single-molecule DNA experiments in micro/nanofluidic devices. On-chip platforms involving slit and channel pores allow precise manipulation of DNA molecules and the optical mapping of the genome^[13]. A key phenomenon observed at confining a linear polymer into a nanochannel of the diameter D is an increase in the longitudinal chain extension (end-to-end distance R_{II}), referred henceforth as the chain pre-stretching. Depending on D , the persistence length P , and the chain width w , the functions $R_{II}(D)$ appropriate for different confinement regimes were established^[4, 5]. The Odijk deflection regime at strong confinement^[14] and the de Gennes blob regime in wide channels^[15] are two ultimate regimes originally proposed. However, most single-chain experiments are carried out at channel confinement between these two classic regimes. For this intermediate region two additional regimes have been later introduced: the backfolding Odijk regime^[16] and the extended de Gennes regime^[4, 5, 13]. Recently, a unified theory was developed that predicts a universal master function $R_{II}(D)$ valid in the wide range of regimes in good agreement with simulations and experiments^[17]. The above theoretical concepts describing the linear chain confinement were later adapted to the confined ring polymers^[5, 6, 18, 19].

In micro/nanofluidic technologies, the confinement effects are often intermingled with the outcomes of the external fields, such as the hydrodynamic flow and electric field. At the external force f the combined confinement/force effect can be envisioned as a “passive” pre-stretching of a polymer by channel

walls complemented by an “active” external deformation. In this notion, the overall change of displacement ΔR at polymer deformation in a channel can be resolved into the contributions due to channel confinement, ΔR_D , and due to external (mechanical) force, ΔR_f [20, 21]. Stretching of linear DNA-like polymers in experiments and simulations revealed that the force-displacement (f - R) functions in slits and channels are considerably affected by the degree of confinement [22-24].

In addition to stretching, the mechanical compression of confined linear DNA molecules below their equilibrium size was explored by using a range of experimental techniques such as movable pistons and funnels [25-27]. An increase in knotting and self-entanglement at the compression of linear DNA was reported in these studies. It is believed that the knot formation in DNA is related to a massive degree of molecular compaction experienced by packed genomes. The blob theory and molecular simulations aid in the explanation of the compression elasticity of confined linear chains. The force-displacement functions f - R for a flexible polymer in a tube of diameter D were deduced using the Flory-type expression of the free energy [28]. The related functions f - S , involving the span S of the molecule, were reported in the simulation study modeling the bacterial chromosome [29]. The study of non-equilibrium piston compression of a strongly confined semiflexible chain in square channels showed the series of chain backfolding into hairpins and the emergence of the organized compressed state [30]. Simulations of the compression/relaxation cycles in the piston setup in a cylindrical channel allow to characterize the self-entanglements arising in linear semiflexible polymers [31]. Furthermore, the piston compression was found to induce a strong tendency for a helical organization in semiflexible polymers confined in a cylinder [32]. Recently, we reported the large differences between the end-chain and piston compression of linear DNA-like polymers [21]. The end-chain compression of moderately confined polymer can be accounted for by the smooth function valid for a Gaussian chain in bulk [33]. Yet, in narrow channels, molecules compressed via end-chains abruptly buckle into hairpins. In contrast, the piston compression of a linear polymer is characterized by a gradual reduction of the chain span S and by smooth f - S functions in the whole range of confinement.

In the present paper, the attention in the compression elasticity of confined chains to the linear polymers is expanded to the ring counterparts. We examine the compression of semiflexible ring polymers under channel confinement and compare their behavior with the analogous linear molecules. The simulation method of moving piston we employed to mechanically compress a polymer closely resembles the nanofluidic experimental technique. We found that chain topology gives rise to several differences in compression elasticity. Primary, the ring polymers are elastically much stiffer at longitudinal compression than the linear analogs. The moderate chain contraction observed at compressive forcing in ring

polymers is in marked contrast with the considerable pliability of linear polymers under the compression. Furthermore, whereas the compression curves f - S of linear molecules show a smooth decrease of the chain span, the compression of ring chains at tight confinement shows an abrupt transition caused by the double-folded ring hairpins. We also found that for both polymer topologies the f - S curves at moderate confinement are correctly described by the mean-field Flory-like theory.

2. Method

The bead-spring discretized wormlike chain (WLC) model described in refs.^[33-36] is used in the Monte Carlo (MC) method to compute the mechanical deformation of confined polymers. A semiflexible polymer is modeled by N partially fused spherical beads connected by effective bonds (characterized by the spring constant). Three contributions to the potential energy are considered, from bond stretching U_{bs} , nonbonded pair interactions between beads U_{nb} , and the bending of two consecutive effective bonds U_b . The bond stretching energy is described by the FENE potential in which the bond length can slightly vary around the preferred length l_0 . The nonbonded interaction of two beads of the diameter w is modeled by the shifted and cut repulsive Morse potential. The diameter w slightly exceeds the effective bond length l because of the weak interpenetration of beads. The penalty for the deviation of a chain from a straight rod is given as $\frac{U_b(\theta)}{kT} = b(1 + \cos\theta)$, where θ is the valence angle between two consecutive bonds in the chain and the parameter b is associated with the chain stiffness.

The identical parameters are assumed in the model for polymers of both topologies. The model polymer consists of $N=300$ beads of the diameter $w = 2.5$ nm. Depending on the chemical structure, one bead may represent typically 5 to 10 monomers. The effective bond length connecting beads $l = \langle l \rangle = 2.34$ nm is slightly lower than the diameter w due to bead interpenetration. The contour lengths of the linear $L_l = (N-1)l$ and ring $L_r = Nl$ molecules are practically the same. The bending energy parameter $b = 20$ should represent the polymers of enhanced chain stiffness typical for helical polymers such as ds-DNA or amylose derivatives. In the WLC model, the parameter b is related to the intrinsic persistence length by $b = P/l$ ^[34,35] from which $P = 46.7$ nm.

The confinement/force effects on the size of linear and ring polymers were monitored through the chain span and the radius of gyration. The mean span S of a molecule is given as its longest dimension along the channel x -axis: $S = \langle S \rangle = \langle \max(x_i) - \min(x_j) \rangle$ where $i, j \in [1, N]$. The span is a common measure of a polymer size in single-chain experiments under confinement. Additionally, the radius of

gyration $R_g = \langle R_g^2 \rangle^{1/2}$ commonly used to assess the polymer size in cyclic chains instead of the end-to-end distance, and its longitudinal (R_{gx}) and perpendicular (R_{gy}) components were also computed. The R_{gy} component was taken as an average of the respective values along the y and z axes.

The confinement of polymers in cylindrical channels is modeled by using a soft-wall potential of the same form as that used for nonbonded repulsive interactions between chain beads. This potential acts between chain segments and walls separated by the cylinder diameter D^* . The accessible volume is thus reduced to an effective diameter $D = D^* - w$ due to wall repulsion.

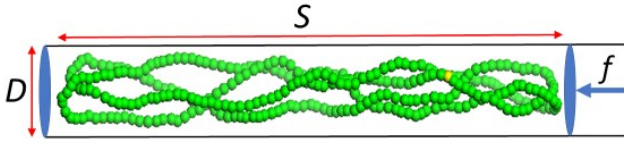


Figure 1. Sketch of the ring polymer compression by the piston and the corresponding simulation snapshot.

The simulation model of polymer compression in a cylindrical channel resembles the nanopiston technique used in experiments (**Figure 1**). The external force f oriented along the piston axis (x -axis) $f = f_x$ is assumed. The compression force $f_x < 0$ modifies the position of a mobile piston that closes the channel from one side, while the other side of the channel is closed by a fixed wall. Both the fixed wall and piston interact with the chain in the same way as the channel walls. The distance of the piston from the fixed opposite wall in the channel is not identical to the chain span S along the channel. In MC simulations, the extra term $dU = -f_x dx_p$, where x_p is the piston displacement, was added to the Metropolis algorithm. Thus we use a constant pressure ensemble (NpT) in which the additional term above represents the volume fluctuation term pdV . For each 20-50 attempted chain moves one piston move was attempted, consisting of a small random displacement of the piston in the neighborhood of its original position. In this move, only the changes in interactions of chain segments with the piston wall are evaluated. Chain moves included the small random displacement of beads and consequential evaluation of change in interactions with all beads and walls. For the random displacement of monomers in rings maximum amplitude of $0.125l_0$ was used to prevent from a bond crossing or a change of topological state of ring and together with nonbonded interaction potential this accounted properly for the excluded volume in ring. For linear chains also reptation was applied as a more effective conformation change attempt.

The constant values of the number of beads $N=300$, the bond length $l = 2.34$ nm, and the persistence length $P = 46.7$ nm are employed in simulation. Hence, the contour lengths of the linear and ring molecules read $L_l = 698.2$ nm and $L_r = 700.6$ nm, respectively. The channel diameter D and the compression force f are two variable parameters. A broad range of the confinement strength is sampled, from the wide channels near the bulk 3d limit ($D/P \rightarrow \infty$) to the narrowest channel of $D \approx 20$ nm ($D/P = 0.44$) near the 1d limit. The compression forces up to $-fP/kT = 40$ (3.55 pN at 300 K) were considered.

3. Results and Discussion

3.1. Piston compression functions

First, the variation of the span with the compression force for the *linear* polymer is presented as a reference (**Figure 2**, the upper panel). For short linear polymers at vanishing compression force, the channel confinement covered in **Figure 2** should involve the sub-persistence (Odijk) regime of strongly confined polymers, the backfolding Odijk regime, and the extended de Gennes regime at moderate confinement. The functions $S(f)$ at $f = 0$ allow to quantify the spontaneous stretching of a polymer on its confinement into a channel of the size D . The non-compressed polymers are pre-stretched in the channel by an amount given by the difference $\Delta S_D = S_o - S_b$, where span S_b refers to the equilibrium size of the unconstrained molecules in bulk ($f = 0$ and $D \rightarrow \infty$) and S_o to their size in the channel at $f = 0$. The pre-stretching ΔS_D , marked in **Figure 2** at the ordinate axis, is always positive and can reach a considerable value in the Odijk regime in narrow channels. The polymer compression described by the curves $S(f)$ brings in the negative force-induced contribution ΔS_f opposing the term ΔS_D . The overall change of displacement ΔS at chain deformation is determined by the sum of the terms ΔS_D and ΔS_f . As expected, plots $S(f)$ show that the span of linear confined molecules diminishes on compression.

Depending on the confinement and force power, various mechanisms of piston compression can be invoked in linear polymers^[23]. At moderate confinement and a weak force, the polymers exist in a disordered coiled state. On increasing the force, the molecules tend by looping to reach more compact, quasi-globular conformations. On the contrary, the polymer compaction under compression in the narrow channels proceeds mainly by hairpin folding. At tight confinement $D/P = 0.44$, the J-shaped end-turns nucleated at weak force $-fP/kT = 1$, develop on stronger compression into the U-shaped hairpins. While the separation of ends in the U-hairpin is near zero, its span is about half of the contour length $S \cong L/2$. The strong compression forces at tight confinement can induce multiple folding of linear chains into

nested hairpins^[30]. Overall, the piston compression behavior of linear semiflexible polymers shown in **Figure 2** concurs with the results reported for DNA-like polymers of $N=1000$ ^[21].

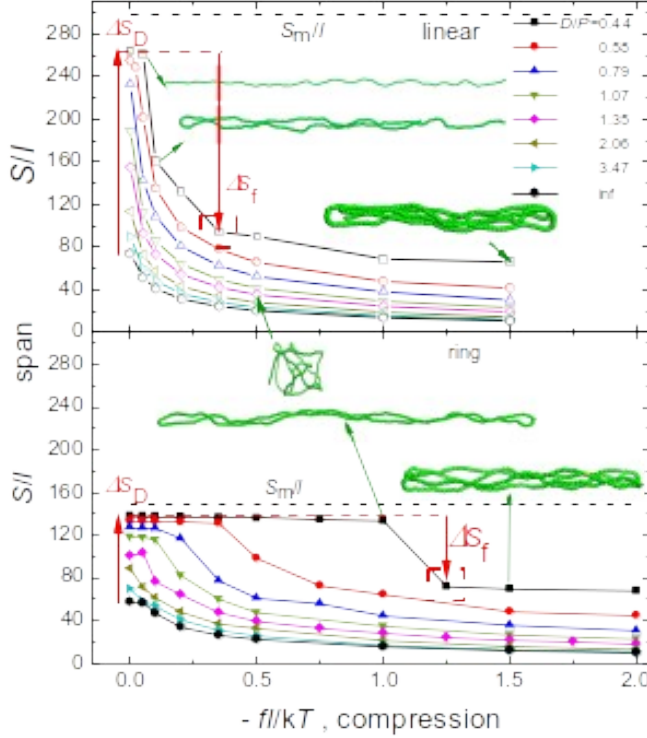


Figure 2. Compression curves span vs force for the linear (empty symbols) and ring (solid symbols) polymers (the upper and lower panel, respectively) at the confinement strengths D/P given in the legend.

The piston compression functions $S(f)$ for the *ring* polymer are presented in the lower panel of **Figure 2** and include the equilibrium span $S_b = 134$ nm of a polymer in bulk. The spontaneous pre-stretching ΔS_D of a non-compressed ring molecule in a channel can be substantial: for example, in the narrowest sampled channel of $D/P = 0.44$, the term ΔS_D amounts to 54% of the maximum achievable extension S_m . Interestingly, even at the compression force $fP/kT = -40$ the negative force-induced contribution ΔS_f is not strong enough to offset the above term ΔS_D .

Several differences in the compression response of linear and ring polymers are notable from the comparison of the upper and lower panels in **Figure 2**. Firstly, the piston squeezing of linear molecules is portrayed by the essentially smooth functions $S(f)$. In contrast, the compression of ring molecules gives rise to the abrupt changes on the curves $S(f)$ in the narrow channels of $D/P < 1$. This phenomenon suggesting the chain folding in ring molecules will be discussed afterward.

Secondly, in the linear chain, a substantial reduction of the span on compression occurs in the region of soft elasticity at forces $f/kT < 0.2$. For example, the full change of the span S/l of a linear molecule on the application of the force $f/kT = -1.5$ in the channel of $D/P = 1.07$ is about 189 (**Figure 2**). However, 66% of this span reduction is already achieved by force $f/kT = -0.2$. Such an area of low resilience to compression is much less articulated in Figure 2 for the ring analog. Put differently, the Hookean spring constant κ_H in the relation $f_H = \kappa_H(S - S_0)$ at the compression of the ring polymer is substantially larger than that of the linear polymer (**Figure 3**). Even in bulk polymers, the constant κ_H (in fN/nm), of about 21 for the ring polymer at the initial phase compression when $\Delta S \cong -75$ nm, is higher by the factor 3.8 than the respective value for the linear counterpart (**Figure 3**, the inset). The difference in the compression stiffness of the ring and linear chains even increases on their confinement in the channel of $D/P = 1.35$.

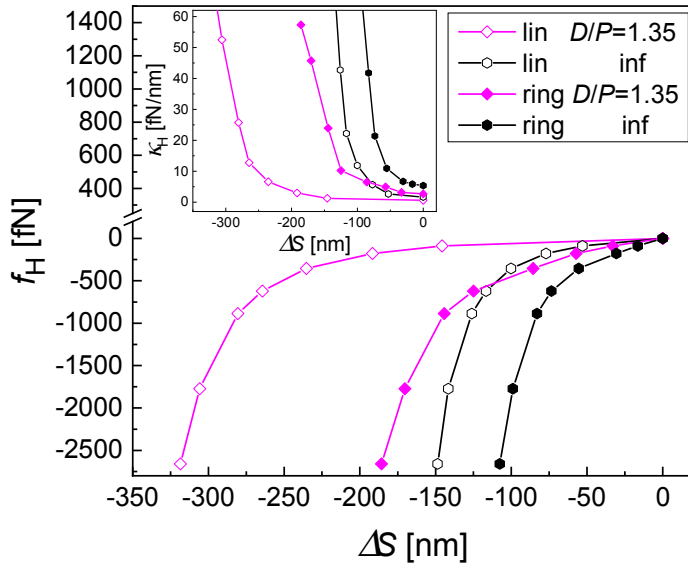


Figure 3. Shortening ΔS of the ring and linear molecules on their compression in bulk and in the channel of $D/P = 1.35$ as the function f_H vs ΔS . The inset shows the respective plots of the Hookean spring constant κ_H .

The difference in the compression response of two chain topologies is linked to the fact, that although they have practically identical contour length L , they differ much in the maximum achievable extension. As seen in **Figure 2**, due to the ring closure constraint, the ring chains show a much lower span than the equivalent linear chains. The maximum achievable extension in a linear chain is $S_m = L_1 = 698.2$ nm, but in a ring chain it is only about half of that value: $S_m = (N-2)l/2 = 347.9$ nm. Hence, the relative

variable S/S_m may provide a more meaningful assessment of compressive squeezing of two polymer topologies.

A comparison of the equivalent curves S/S_m vs fP/kT in **Figure 4** clearly shows a predisposition of the ring chains to attain a higher relative extension than the linear ones. For example, the relative equilibrium span S_b/S_m of the linear and ring molecules at $f=0$ in bulk is 0.25 and 0.39, respectively. In a similar correspondence, 88% and 93%, is the respective relative extension at $f=0$ in the channel of $D/P = 0.44$. The predominance in the relative extension of the ring chains relative to the linear ones is maintained in Figure 4 in the whole range of the compressive forcing. In addition to the functions $S(f)$, the piston compression functions $R_g(f)$ based on the radius of gyration were also computed. The $R_g(f)$ functions resemble those in **Figures 2** and **4**, just the distinct features accompanying the ring polymer compression are less pronounced (**Figures S1** and **S2** in Supplementary Information).

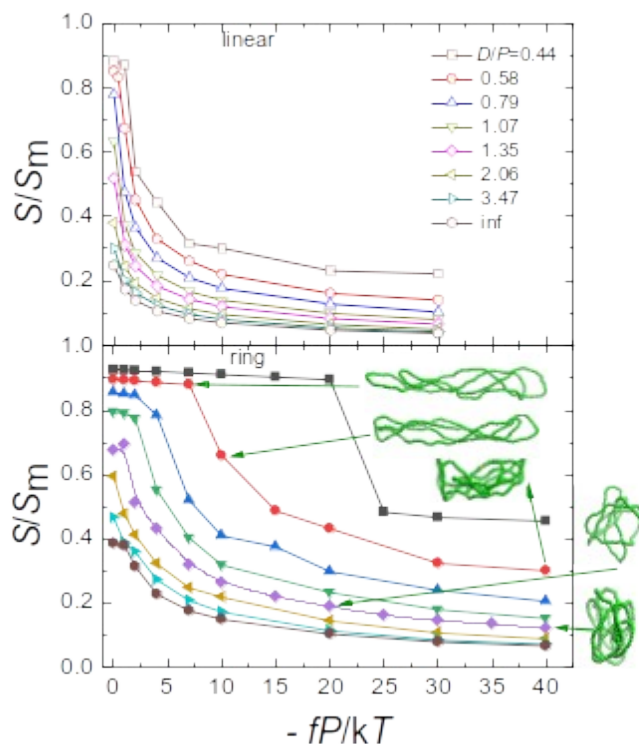


Figure 4. The reduced span of linear and ring macromolecules as a function of the compressive force for the different degrees of confinement given in the legend.

The higher relative extension of the ring chains relative to the linear ones shown in **Figure 4** corroborates a popular conjecture^[5, 6, 9, 18, 19] that a confined ring polymer can be viewed as a parallel juxtaposition of two linear subchains. Each subchain is effectively constrained to the channel of the diameter D_{eff} diminished relative to D for the linear polymer. It is assumed that the reduced channel exhibits half

of the cross-section area of the original channel, that is, $D_{\text{eff}} = D/\sqrt{2}$. The excluded-volume repulsion of the subchains on their confinement in a channel gives rise to the chain pre-stretching that is much higher in the ring molecules than in the linear ones. However, a representation of a semiflexible ring polymer in a channel by two linear subchains may not be entirely applicable to the circular DNA molecules such as plasmids. An important property of double-stranded DNA is a spontaneous twisting of the duplex into a supercoiled conformation in which the molecule is wound around itself and forms a higher-order helix. The supercoiling is strongly affected by the confinement of circular DNA molecules in a channel^[37] and may be further enhanced by compression^[32]. However, the results in **Figures 2-4** are in all aspects relevant to the nicked circular DNA without supercoiling. A nick is a discontinuity in DNA molecule that allows DNA strands to untwist and release the torsional energy^[38, 39]. Nicking can result from biological processes in the cell or from DNA damage.

3.2. Chain folding in ring polymers

As in linear molecules, the mechanism of compressive compaction of ring polymers shown in **Figures 2 and 4** much depends on the strength of confinement and the external force. Confinement hinders looping and folding in the ring chains induced by thermal energy and compression force. At moderate confinement $D/P = 2.06$ the randomly coiled ring chains gradually develop on mild compression into more compact anisotropic conformations. The subsequent compression results only in a minor additional contraction of ring molecules (see snapshots in Figure 4). However, in channels of $D/P < 1$, the weak compressive forces are insufficient to overcome the energy barrier to folding and the span remains steady. Once the critical force f_{cr} is reached, the function $S(f)$ displays an abrupt drop of the span (**Figures 2 and 4**). The critical force $f_{\text{cr}}P/kT$ needed to induce the compression transition increases (in the absolute value) on narrowing the channels, from about -2.5 at $D/P = 0.79$, to -8 at $D/P = 0.58$, and -22 at $D/P = 0.44$. **Figures 2 and 4** suggest an occurrence of a small critical force ($f_{\text{cr}}/kT = -1.5$) also in the linear molecule in the narrowest channel.

The sharp downturn of the span of ring molecules in narrow channels in **Figures 2 and 4** can be taken as an explicit signal of the folding events. For the channel size $D/P = 0.44$, it is possible to identify the specific configurations of ring structures engaged in the compression transformation. The non-compressed ring molecules in the Odijk regime are highly extended, to 93% of its maximum span S_m . The extended polymer is converted by the critical compression force $f_{\text{cr}}P/kT = -22$ into a hairpin-like structure by double-folding the molecule roughly in the middle. In this compression transformation the rela-

tive span S/S_m changes from 0.90 to 0.48 (**Figures 2 and 4**). The demands on the bending energy and available space at chain folding are much higher for the ring molecules than for the linear ones. Correspondingly, the critical force $f_{cr} = -1.95$ pN at 300 K for the formation of the hairpin-like structure with two folds and four parallel subchain strands in ring molecules is much stronger than of making a standard hairpin with two parallel strands in the linear ones ($f_{cr} = -0.13$ pN). The latter value well compares with an estimation $f_{cr} = -0.22$ pN using the analytical model of ref. ^[19], Equation A3, for the folding/unfolding force in a simple hairpin of a linear molecule.

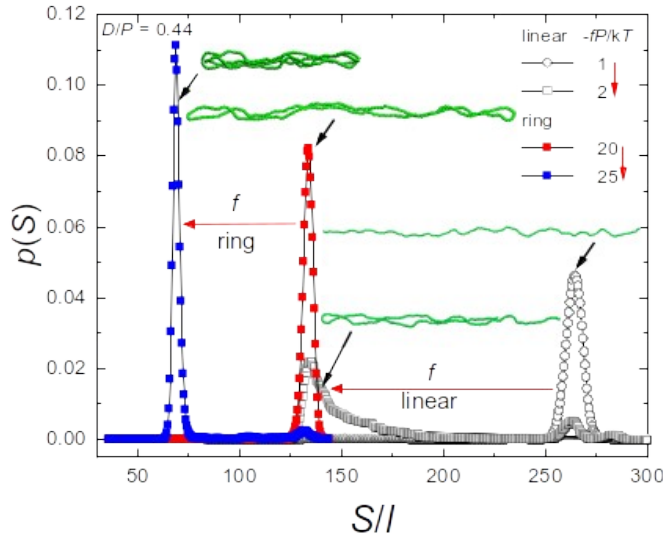


Figure 5. The distribution functions $p(S)$ of linear and ring polymers confined in a narrow channel of $D/P = 0.44$ compressed by the force given in the legend.

The interpretation of the abrupt changes in the functions $S(f)$ as folding events is validated by other simulation data. The distribution function $p(S)$ computed for a ring molecule confined at $D/P = 0.44$ shows the narrow distribution peaked at $S/l = 132$, confirming that the molecule remains highly extended even at the compression force $fP/kT = -20$ (**Figure 5**). Yet, at a slightly stronger force $-fP/kT = 25$, a novel narrow peak associated with the folded ring molecule occurs, located at about half of the mentioned value of S/l . An analogous shift of peaks of the function $P(S)$ for $D/P = 0.44$ is also observed in **Figure 5** for a linear chain. In that case, the larger width of the right-most peak at $-fP/kT = 1$ indicates a presence of multiple fairly extended conformations. At slightly stronger compression of $fP/kT = -2$, this peak moves to $S/l = 135$, to the location of the peak of an extended ring molecule. Thus, the extended linear polymers convert primarily into the U-turn hairpin along the line $L \rightarrow L/2$. However, a broad shoulder of the latter peak suggests the presence of a variety of other hairpin-like structures.

The orientational correlation functions provide another validation of the association of the sudden changes in the functions $S(f)$ with the ring folding. In bulk semiflexible chains the average tangent-tangent correlation function along the short arc length s decays exponentially with their separation: $\langle C(s) \rangle = \langle \mathbf{u}(i) \cdot \mathbf{u}(i+s) \rangle = \langle \cos \theta(s) \rangle = \exp(-s/P)$ [7, 8, 10]. The unit vectors $\mathbf{u}(s)$ tangent to the chain are at positions i and $i + s$, respectively, with i covering the interval from 0 to $L - s$. The correlation function $\langle C(s) \rangle$ provides a base for the determination of the orientational persistence length P . It is well-known that the chain topology, stiffness, and confinement is in a sensitive manner reflected in the shape of the function $\langle C(s) \rangle$ [8, 40-42]. Instead of the exponential decay, the correlation functions of ring chains exhibit the regions where $\langle C(s) \rangle$ is negative [7, 8, 10]. The function $\langle C(s) \rangle < 0$ conveys a tendency to the opposite orientation of bonds separated along the arc. In ring molecules this anti-correlation effect is a direct consequence of the chain-end closure.

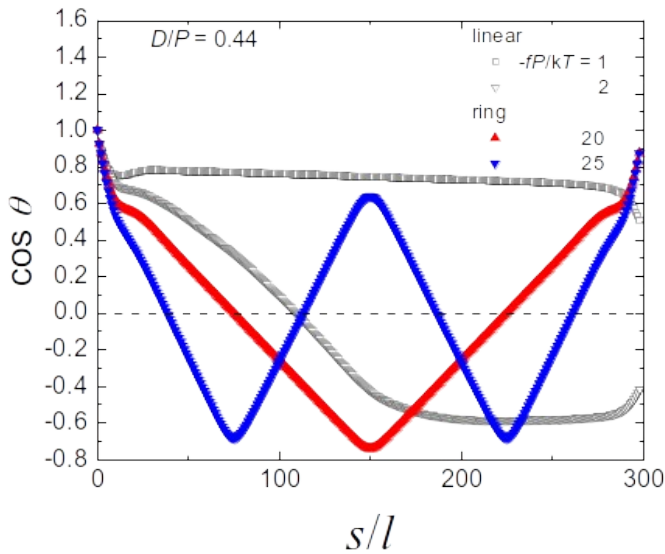


Figure 6. The plots of the orientational correlation function $\langle C(s) \rangle$ of the confined linear and ring polymers in the channel of $D/P = 0.44$ under the compressive force fP/kT given in the legend.

The functions $\langle C(s) \rangle$ for the compressed polymer confined in the channel of $D/P = 0.44$ are shown in **Figure 6**. The identical initial slopes of all curves confirm that the local stiffness of linear and ring chains is the same. At larger s/l the overall structure develops and can be analyzed. The function $\langle C(s) \rangle$ for a ring polymer subjected to the force $fP/kT = -20$ corresponds to the correlation behavior of a highly extended ring molecule. The positive correlations along the first subchain gradually decrease and reach the negative region of $\langle C(s) \rangle$. After the U-turn halfway in the ring at $S/l = 150$, the correlations along

the second subchain increase. An analogous, perfectly symmetrical curve $\langle C(s) \rangle$ characterizes in Figure 6 the ring molecule under force $fP/kT = -25$, after the folding transition. However, this time the function $\langle C(s) \rangle$ showing three extrema at typical distance $s/l = 75$ describes the orientation correlations along a double-folded molecule of four parallel ring strands.

The correlation functions $\langle C(s) \rangle$ for the linear chain are also included in **Figure 6**. The function $\langle C(s) \rangle$ representing the straight conformation under tight confinement and $fP/kT = -1$ displays after the initial decay a distinctive minimum and a long plateau. A strong tendency of segments to align with the channel axis in the Odijk regime secures a high directional correlation to very large separations. In contrast, the $\langle C(s) \rangle$ function of a linear polymer under the stronger- than-critical force $fP/kT = -2$ in **Figure 6** shows a region of the negative values, typical for the folded conformations. The lack of symmetry of the latter function affirms an occurrence of many hairpin-like structures upon induced folding referred to in **Figure 5**.

On widening the channel, but still within the Odijk regime of $D < P$, the sharp breaks in the compression functions become less conspicuous. The absolute value of the critical forces diminishes, as in wider channels the smaller stored elastic energy is needed to compensate for the energy cost of chain reversal. In channels of this size, the compression transitions are associated with the multiple folding events in a large number of conformations characterized by the broader distribution functions $P(S)$ than those shown in **Figure 5**. Eventually, at moderate channel widths, the distribution functions $P(S)$ at compressive forcing are quite wide, in conformity with the abundant folding and looping occurring in ring molecules. Accordingly, the compression functions in **Figures 2** and **4** show a smooth shape characteristic for a process of gradual compressive compaction of polymers.

The data suggest that the linear and ring molecules share a similar pattern of the compression transformation. In narrow channels, the contraction proceeds for both topologies by folding the molecule roughly in the middle. The sharp character of this process in the tightly confined molecules is a distinctive behavior reminding the buckling transition^[43, 44]. Many technological and biological phenomena are based on the controlled buckling of ring objects when under compressive loads. In general, the buckling instabilities in rigid beams arise since it is energetically more favorable for the structure to bend, and thus balance the applied load without increasing the internal stress. Analytical arguments revealed that confinement by a spherical shell can induce buckling in semiflexible polymer rings^[43]. Our data corroborate this type of elastic response also for tube-like confinement where polymer rings assume the shape of prolate ellipsoids. The ring polymers sustain quite larger forces before buckling when compared to linear chains, since their effective confinement is much tighter than that of linear analogs. The linear chains

will feature essentially the same behavior when smaller channels or chains of higher stiffness are considered.

An adequate effective stiffness of a chain is a crucial prerequisite for an occurrence of polymer buckling under confinement. This is documented by comparison of the behavior of semiflexible and flexible polymers **in Figure S3** in Supplementary Information. The compression of a flexible ring polymers results in a smooth curve $S(f)$ without any indication of an abrupt change.

3.3. Confinement regimes

The functions $S(f)$ discussed so far define the response of confined ring polymers to the compression force. A related response of polymers to confinement is specified by the function $S(D)$ for the dependence of the span on the channel width. Both kinds of functions represent the cross-sections of the hypersurface $S(D, f)$ conveying how the span is influenced by the combined confinement/force constraints (**Figure S4** in Supplementary Information).

The current theories of polymers under confinement do not encompass the external force. However, the confinement functions in the absence of the force $S_0(D)$ are comprehensively detailed by experiments, theory, and simulations primarily for linear chains^[4, 5, 13]. Due to the interplay of different length scales, several confinement regimes can arise along the curve $S_0(D)$ in the examined polymers. The strongly confined chains are described by the Odijk theory of rigid segments that deflect back and forth from the channel walls^[14]. Confinement near the persistence length ($D \sim P$) is described by the back-folded Odijk regime^[16], where the excluded volume repulsion between deflection segments makes the chain to fold back. The extended de Gennes regime at moderate confinement describes^[4, 5] the chain statistics over the range $P < D < P^2/w$.

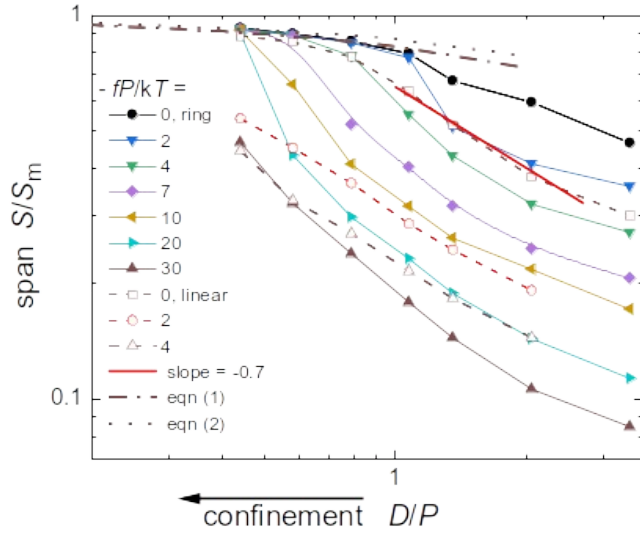


Figure 7. The logarithmic plot of the reduced span of ring molecules subject to a range of compressive forces given in the legend as a function of the reduced channel width D/P . The dashed lines show the related plot for linear polymer.

No rigorous theory has yet been derived for the dependence of the span on the channel size for the ring polymers confined in channels. We use the current practice of viewing a ring polymer as a parallel connection of two linear chains to elucidate the computed functions $S(D)$ (**Figure 7**). Three mentioned linear-chain regimes, the Odijk, backfolded Odijk, and extended de Gennes ones, can also be envisaged for ring molecules. The uppermost curve in **Figure 7** represents the reference function $S_0(D)$ at vanishing force. The compression forces induce a downward shift of the confinement curves in **Figure 7** to the smaller spans. At strong compression, the reduction of the span is substantial: the force-induced contribution ΔS_f prevails over the span gain ΔS_D due to pre-stretching by a channel.

The region of narrow channels in **Figure 7**, where D is smaller or comparable to P corresponds in non-compressed linear molecules to the classic Odijk regime, and to the backfolding regime. The mean extension R_0 of a linear polymer in the classic Odijk regime is given by

$$R_0 = L[1 - A(D/P)^{2/3}] \quad (1)$$

where $A = 0.1701$ was calculated for a cylindrical channel^[45]. The generalization of Equation (1) to ring polymers employs the construct of two linear subchains trapped in a channel of effective diameter reduced to $D/\sqrt{2}$. Then, the mean extension R of a ring molecule in the reduced channel lumen reads

$$R_o = (L/2)[1 - A(D/P\sqrt{2})^{2/3}] \quad (2)$$

The behavior of chains of both topologies in narrow channels is compared with predictions of the Odijk theory in **Figure 7** on the assumption that the mean extension R can be represented by S . In non-compressed molecules the decrease of the span on the channel widening is slower in ring molecules than in the linear ones, in qualitative accord with the predictions by Equation (1) and (2). Thus, the Odijk regime is broader in ring polymers than in the linear ones, as observed earlier^[8]. However, the decrease of curves S_o/S_m in **Figure 7** is for both topologies more pronounced than predicted by the theory. This suggests an emergence of the backfolded regime associated at $f=0$ with the thermally-induced folding of chains into hairpins. As expected, the backfolding is more intense in the linear chains than in ring ones.

Furthermore, the curves $S(D)$ at two weak forces $fP/kT = -2$ and -4 can be compared in **Figure 7**. The decrease of span (relative to that for $f=0$) on channel widening in these curves is much larger in linear polymers than in the ring counterparts. The span reduction comes mainly from the compression-induced backfolding, more robust in the linear chains. The recent simulation of confined linear polymers suggests that compression proceeds by folding the chains into the nested S-shaped hairpins that ultimately give rise to an organized compressed state^[30].

Understanding of the backfolding in confined ring polymers, and of the associated confinement regime, has remained far behind the progress for linear polymers. The double-folded conformations are conjectured in the concentrated and entangled solutions, gels, and melts. These dense assemblies of polymers in bulk can be treated as the confinement of a ring molecule in an array of fixed obstacles^[46, 47]. Under such confinement, an increase in polymer length promotes folding and interpenetration of rings^[47]. The curved double-folded conformations were also observed in AFM experiments with the two-dimensional systems of deposited DNA plasmids under circular confinement^[48]. For DNA-like ring polymers confined in a cylinder, a helical organization of chains was reported at moderate compression^[32]. Yet, under strong compression, the backfolding of ring polymers was detected^[32]. However, the generation of double-folded conformations by buckling described above was not yet reported.

The compression-induced folding may modify the boundaries of the confinement regimes assigned in the absence of force^[20]. For example, the size of the classic Odijk regime along the $S(D)$ functions in **Figure 7** diminishes on compression, as the crossover to the backfolded regime moves much below D/P

= 1 for both chain topologies. Ultimately, at compression of a ring molecule by the forces $fP/kT = -30$ and stronger, the classic Odijk regime completely vanishes due to the complete folding of a molecule.

Finally, the extended de Gennes regime in $S(D)$ plots in **Figure 7** can be treated by the blob scaling theory of confined polymers^[15]. In the blob theory, a chain in a tube of diameter D is viewed as a string of self-avoiding blobs of size D linearly arranged along the tube axis. The competition of the length D with the length scales P and w determine the polymer behavior expressed by a scaling relationship such as $S_0 \sim aD^{-x}$ where a is the numerical prefactor. The large contour lengths are usually needed to establish the power-law exponents x in the individual confinement regimes^[4, 5]. In the simulation of sufficiently long chains, the same exponent $x \cong -0.7$ was found in the extended de Gennes regime for DNA-like polymers of both linear and ring topologies in absence of supercoiling^[9, 49]. The exponent x approximately inferred from a short quasi-linear section of the function $S_0(D)$ in **Figure 7** seems of a comparable value. The analysis of a combined operation of confinement and compression in the $S(D)$ curves in **Figure 7** is beyond the present limits of the scaling approach to confined polymers.

3.4. Flory-type theory

The Flory-type mean-field expression for the free energy is a popular tool to calculate the size of a self-avoiding chain^[4, 5, 28, 29]. This scheme combined with the blob scaling approach was applied to the polymers confined in a cylinder and to predict their size as a function of channel size and the external force^[28]. In the following, the simulation dependences $S(D)$ and $S(f)$ in the extended de Gennes regime are analyzed by this approach.

The free energy of the linear flexible chain confined in a cylinder when $f = 0$ is given according to renormalized Flory theory as^[28]

$$F = A \frac{R^2}{(N/g)D^2} + B \frac{D(N/g)^2}{R} \quad (3)$$

where A , B are constants and g represent the number of chain segments in one blob with the size of the channel diameter D , while the extension of the whole chain is $(N/g)D$. An assumption of the Flory exponent $\nu = 3/5$ in the relation $R_F \sim N^\nu$ for the excluded volume within each blob gives $D \sim g^{3/5}$. By minimizing the free energy F , the equilibrium chain extension of linear chains along the channel is obtained^[28] $R_0 \sim ND^{-2/3}$. To adopt this approach to wormlike polymers, the persistence length is incorporated into the

above relations. Then for the semiflexible chain in blobs $D \sim g^{3/5} P^{1/5}$ and the chain extension is $R_0 \sim ND^{2/3} P^{1/3}$.

In an adaptation of Equation (3) to ring polymers, the scheme^[5, 6, 9] of two parallel subchains placed in an effective channel of the diameter $D/\sqrt{2}$ is used. Then the free energy of a wormlike ring polymer in a cylinder when $f=0$ is given^[6]

$$F = 2\zeta + B(D/\sqrt{2})\zeta\zeta \quad (4)$$

Again, a consideration of the excluded volume in each blob of the semiflexible ring chain yields $D/\sqrt{2} \sim g^{3/5} P^{1/5}$. This leads to the equilibrium extension $R_0 \sim 2^{-2/3} ND^{2/3} P^{1/3}$.

It is seen that the Flory-type theory in the extended de Gennes regime in the absence of the compression force predicts for linear and ring polymers the identical power-law exponent $-2/3$ for the dependence of the mean extension R on the channel width D . When the more precise value of the Flory exponent $\nu = 0.588$ is used, the scaling exponent $x = -0.7$, in agreement with the simulation data for DNA-like polymers^[49]. The theory also predicts that the ring polymer extension R_0 is by the constant factor $2^{-2/3} = 0.63$ smaller than the linear polymer extension regardless of the channel width.

The great benefit of the Flory scheme is that it allows an assessment of the force required to extend or to compress a polymer confined in a channel, that is, in our case, of the function $f(S)$ for a given channel width D . The external force is determined from the derivation of the free energy $f = \partial F / \partial R$. The following force-displacement relation $f(R)$ is obtained for linear polymers^[28]

$$f_l P / kT = (P/D)[R/R_0 - (R/R_0)^2] \quad (5)$$

where the condition that $f=0$ for $R = R_0$ is used, leading to $2A=B$, and this spring constant is set to kT . In analogy, for the ring polymers, we obtain

$$f_r P / kT = 2^{3/2}(P/D)[R/R_0 - (R/R_0)^2] \quad (6)$$

Notice that the equilibrium extension R_0 at zero force at given D for the ring chain is different from in the linear chain.

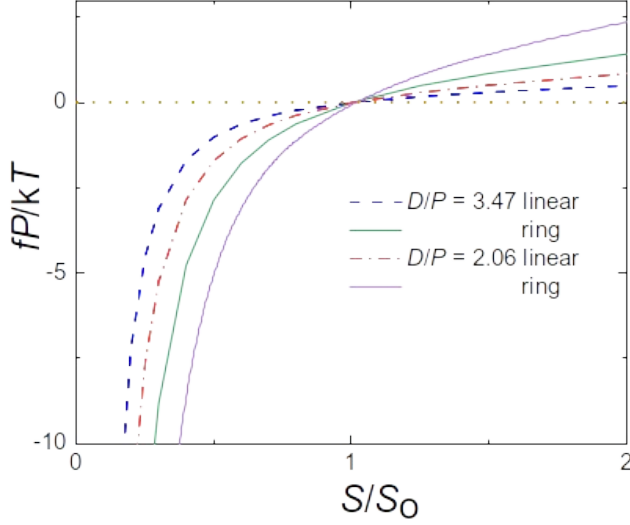


Figure 8. The functions $f(S)$ in the extension and compression range predicted by Equation (5) and (6) for the linear and ring polymers confined in the channels of $D/P = 2.06$ and 3.47 .

The above relations f - R should be universally valid for the deformation of confined polymers in the extended de Gennes regime. They predict that the ring polymer is stiffer than the linear one by the numerical factor $f_r/f_l = 2^{3/2} = 2.83$. It is well known that semiflexible chains show weak excluded volume and tend to be ideal for not very long chain lengths. Interestingly, the same f - R relation, Equation (6), holds if we consider the ideal wormlike chain within blobs in the ring in Equation (4), namely $(D\dot{\epsilon}\sqrt{2})^2 = 2gIP$. Thus, the f - R relation in Equation (6) remains the same, only the reference extension for the ideal ring chain changes to $R_o \sqrt{2}(NIP/D)$. In application of theory to the simulation data we use the chain span S instead of R in the above relations.

The functions $f(S)$ from Equation (5) and (6) for the linear and ring polymers confined in channels of two sizes are plotted in **Figure 8**. The plots comply with the ratio $f_r/f_l = 2.83$ and endorse the higher elastic stiffness κ of the ring polymers both at the extension and compression relative to the linear counterparts, in agreement with data shown in **Figure 3**. Earlier, the ratio $\kappa_r/\kappa_l = 4.5$ for the effective spring constants of ring and linear polymers was derived using the Flory scheme^[6]. One should note that the spring constant κ is a measure of the chain stiffness differing from the persistence length P . The spring const κ quantifies the response of a polymer to the deformation by an external force, whereas P accounts for the “static” chain stiffness.

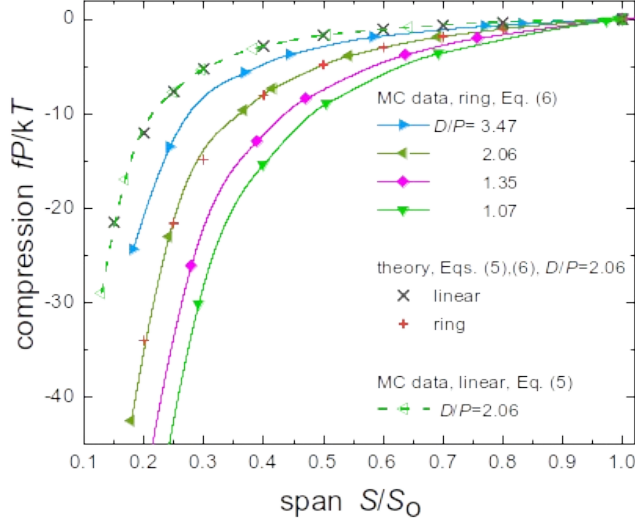


Figure 9. Comparison of the force-compression functions $f(S)$ from the simulation (solid symbols) with Equation (6) (full lines) for the ring polymers confined in the channels given in the legend. Additionally, the data for the linear chain at $D/P = 2.06$ from the simulation and Equation (5) (dashed line) are included. The crosses (+), (x) represent the respective predictions of Equation (5) and (6) without using the MC data for f , S and S_0 .

The force-compression data $f(S)$ from a simulation of confined ring chain are recast into the form that allows the comparison with Equation (6) (**Figure 9**). It is seen that the Flory theory very well reproduces the simulation data of ring polymers in the extended de Gennes regime, and at $D/P = 1.07$, probably even in the backfolded regime. The agreement of simulation and theory is confirmed in **Figure 9** also for the linear polymer in one channel size. The power of the Flory scheme to predict the compression of linear polymers at moderate channel confinement was noted previously^[28, 29]. Our data validate that this strength of the theory applies as well to the ring polymers.

The general success of the original Flory scheme for the free energy of a linear chain is often ascribed to a unique cancellation of errors. This assertion may be relevant also in the case involving the elastic term in Equation (3) at polymer compression. The first term in Equation (3) describes the elastic entropy of a polymer made of linear series of blobs behaving like an entropic spring. The second term describes the mutual exclusion between neighboring blobs. However, the elastic free energy much depends on the condition of which variable is held fixed or allowed to fluctuate^[50, 51]. Moreover, the different expressions apply to the elastic free energy in the compression and stretching regime. The term used in Equation (3) is appropriate only for the end-stretching of polymers by the constant force in the Gibbs

ensemble^[33]. Instead, the scalar Helmholtz ensemble is more fitting to portray the deformation of a polymer with unconstrained ends^[50, 51]. Several force-displacement relations describing the compression of DNA in bulk in such a situation were examined^[33]. The proper approximate formula for the elastic free energy of a polymer with free ends, valid for both extension and compression, reads^[52]

$$F/kT = \beta[(R/R_0)^2 + (R_0/R)^2] \quad (7)$$

In the Flory-like theory, Equation (3), the elastic energy is represented only by the first term of Equation (7). The second elastic term of Equation (7), essential at compression, is missing, and seems to be effectively included in the second, excluded-volume term of Equation (3).

3.5. Shrinking factor

The difference in the chain size between the linear and the ring polymer topology is conventionally expressed by the shrinking factor^[53]. This geometric factor is most often defined as the ratio of the mean-square of the radii of gyration $G = (R_g^2)_r / (R_g^2)_l$ of the ring and linear chains. For ideal Gaussian chains $G = 0.5$. To analyze the effect of the chain architecture on the size of confined and compressed polymers (**Figure 10**) instead of G we use the index $g = S_r/S_l$, defined for the span. Bear in mind that the shrinking factor, traditionally denoted by g , differs from the number of chain segments in one blob g discussed earlier.

For the reference state of the bulk non-compressed polymers, the simulations predict the factor $g_0 = 0.780$ (**Figure 10**). This value concurs with the value of $g_0 \cong 0.8$ ^[7] for a wormlike chain of $P/L = 15$, the same as in the present model. The recent theory^[54] based on the Flory approach provides $G_0^{1/2} = 0.758$ for the flexible chains in bulk, in harmony with many theoretical and simulation results for polymers in good solvents. Excluded volume interaction and chain stiffness contribute to an increase in the shrinking factor relative to the value $G_0^{1/2} = 0.707$ for the ideal chains. Besides, one should note that the span-based shrinking factors show higher values than those based on the radius of gyration^[53].

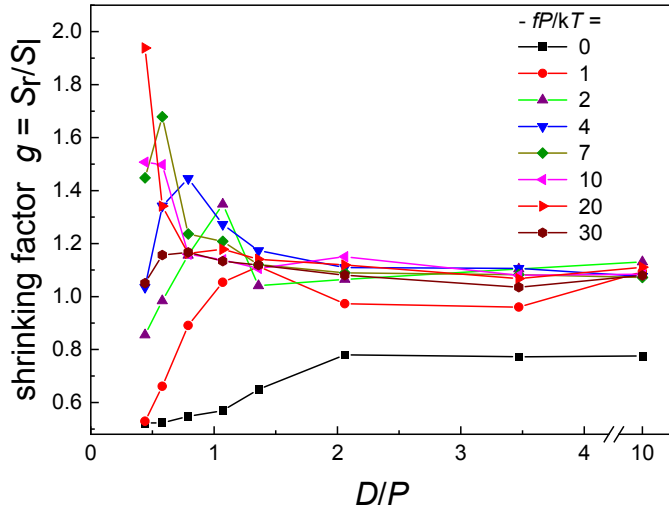


Figure 10. Variation of the shrinking factor g with the channel size D/P at the compressive forces fP/kT given in the legend.

The dependence of the g -factor of semiflexible polymers on the channel size in the absence of compressive force is given by the lowest curve in **Figure 10**. On shrinking the channel size, the g -factor maintains down to about $D/P = 2$ at moderate confinement the value $g_0 = 0.780$ for polymers in bulk. Then, in the domain of the backfolded and classic Odijk regime, the function $g(D)$ drops, and in the narrowest channel reaches $g = 0.522$ (**Figure 10**). As expected, the size of highly extended ring chains at tight confinement and zero compression is about one-half of that of linear chains.

Qualitatively, the independence of the shrinking factor from D at moderate confinement in **Figure 10** concurs with the constant value $g = 0.63$ predicted by the Flory theory, as mentioned earlier. The disharmony of the two latter values may be related to the difference between S and R variables. Strictly speaking, the chain extension R in Equation (3) corresponds to the Flory extension R_F , defined by the maximum of the radial distribution function $P(R)$. In the simulation of the flexible chains in cylindrical channels^[9] the constant $g = 0.584$ was reported for the whole range of the channel widths. The above value was even reduced to about 0.5 by increasing the chain stiffness by way of the bending potential^[9].

The piston compression of confined polymers brings two marked changes in the functions $g(D)$. At first, the plateau of a roughly constant shrinking factor raises from 0.78 to $g \cong 1.1$, that is, the span of the compressed ring molecules at moderate confinement is larger than that of the linear one. Merely the weak force $fP/kT = -2$ is sufficient to realize such a raise of the plateau in the function $g(D)$. The values of the factor g larger than unity are a consequence of the behavior shown in **Figure 2** that the linear

polymer more readily adapts its shape to the piston compression than the stiffer ring analog. Secondly, the functions $g(D)$ of compressed polymers exhibits a peak in the narrow channels. For the weak force of $fP/kT = -2$ the peak is located at about $D/P = 1$. Then, the peak moves to smaller channels on stronger compression, and eventually, the peak vanishes. This non-monotonous shape of the function $g(D)$ is an outcome of compression transitions that proceed in the chains of both topologies. In a linear polymer, the weak compression may be sufficient to induce the hairpin folding and chain shortening in narrow channels. However, the span of the ring polymers is much less affected by weak forces. As a result, the factor g raises at tight confinement with the force (**Figure 10**). Ultimately, at f_{cr} , the energy demand to double-fold the ring conformation is reached, and the ring polymer also shrinks, and the g factor drops.

The g -factor is used to evaluate the “excess” elongation per unit length of the ring molecules in channels due to their higher contour density and greater self-interaction, as compared to the linear counterparts. Accordingly, in the case of two overlapping subchains of a ring in a channel, each has a larger extension than in the absence of the other. Thus, the factor $g = 0.780$ for non-compressed polymer in the channel of $D/P = 2$ implies that the ring molecule of the length $2N$ is 56 % more extended than its linear counterpart of the length N . In the narrow channel of $D/P = 0.44$ this excess extension of a ring polymer is only 4.4 %.

4. Conclusion

We have investigated in simulations the compression of ring wormlike polymers by a moving piston in a cylindrical channel. Jointly with the parallel data for linear polymers, the effect of chain topology on compression elasticity of relative stiff polymers such as dsDNA or helical polysaccharides can be assessed. For a polymer under the combined confinement/compression effect, we resolve the chain span S into contributions due to a “passive” pre-stretching of a polymer by channel walls, and due to an “active” deformation by the compression force f . Simulation reveals that the confinement pre-stretching, quantified by the term ΔS_D , may in narrow channels offset the span reduction due to the force-induced term ΔS_f .

The dependence of the span S on the force f shows that ring polymers are considerably more elastically stiff at longitudinal compression than the linear analogs. At moderate confinement, the size contraction at compressive forcing is modest in ring polymers, whereas a considerable shortening takes place in linear polymers. The difference in the compression behavior arises mainly owing to the much stronger effective confinement of two parallel subchains of a ring molecule in a channel relative to that

of a single-chain linear polymer. The excluded-volume repulsion of two subchains gives rise to the enhanced pre-stretching of ring molecules (relative to the linear ones) on their confinement in a channel.

The compression curves $S(f)$ of linear polymers predict for a linear polymer a smooth decline of the span and chain contraction by looping and folding. In contrast, the curves $S(f)$ in ring polymer show a sharp drop of the span at tight confinement. This abrupt transition is interpreted as the buckling of a ring polymer from an extended conformation into a double-folded hairpin. The shape transition occurs at the critical (Euler) force f_{cr} sufficient to overcome the hindering energy barrier of channel walls. The critical force f_{cr} at tight confinement observed in the ring polymer is about an order magnitude larger than that in the linear chains. The distribution function of the span $P(S)$ and the orientation correlation function $\langle C(s) \rangle$ of chain segments assist in explaining of the mechanism of polymer contraction induced by force. For both topologies, the size reduction proceeds by folding the molecule roughly in the middle. The shrinking factor g defined by the ratio of sizes of the ring and linear chains shows a complex dependence on the channel width and force, much differing from the existing results.

Furthermore, the variation of the chain span with the channel width under the range of the compressive forces is presented. Such functions $S(D)$ are not yet presented in experiments or considered in the scaling theory of confined polymers. Simulations show that the compressive forcing may modify the conventional boundaries of the confinement regimes. For example, the size of the classic Odijk regime diminishes on compression because of extensive backfolding. On the other hand, our data validate that polymer compression under moderate confinement is well described for both topologies by the mean-field Flory scheme. The simulation predicts the higher elastic stiffness of ring polymers at deformation relative to linear counterparts, in the excellent agreement with the theory.

The above findings should be of assistance in interpretation of the compression behavior of DNA-like ring polymers under spatial constraints such as in nanofluidic experiments, disordered media, or crowded environments. The results are also relevant to the circular DNA involving nicks that allow to untwist DNA strands. Our data confirm that compression of ring polymers in a channel promotes looping and backfolding in molecules. Such chain-ends motions pave the way to the chain knotting typical for DNA in many biological systems. In linear DNA, the compression experiments in nanochannels discovered an enhanced population of knotted molecules^[27]. In ring polymers, knotting under the combined action of confinement/force was explored for the slit/stretching pair^{[55][52]}. The impact of the compression on the knot formation in the channel-confined ring polymers remains an intriguing theme for further experimental and simulation study^[31].

Supporting Information

Supporting Information is available from the Wiley Online Library or the author.

Acknowledgments

This work was supported by the grant SRDA-15-0323 and VEGA 2/0102/20. Furthermore, the authors would like to acknowledge the contribution of the COST Action CA17139.

Conflict of Interest

The authors declare no conflict of interest.

References

- [1] F. M. Haque, S. M. Grayson, *Nat. Chem.* **2020**, *12*, 433.
- [2] X.-Y. Tu, M.-Z. Liu, H. Wei, *J. Polym. Sci., Part A: Polym. Chem.* **2016**, *54*, 1447.
- [3] A. Ryoki, H. Yokobatake, H. Hasegawa, A. Takenaka, D. Ida, S. Kitamura, K. Terao, *Macromolecules* **2017**, *50*, 4000.
- [4] L. Dai, C. B. Renner, P. S. Doyle, *Adv. Colloid Interface Sci.* **2016**, *232*, 80.
- [5] B.-Y. Ha, Y. Jung, *Soft Matter* **2015**, *11*, 2333.
- [6] Y. Jung, C. Jeon, J. Kim, H. Jeong, S. Jun, B.-Y. Ha, *Soft Matter* **2012**, *8*, 2095.
- [7] Z. Benkova, P. Cifra, *Macromol. Theory Simul.* **2011**, *20*, 65.
- [8] Z. Benková, P. Cifra, *Macromolecules* **2012**, *45*, 2597–2608.
- [9] J. Sheng, K. Luo, *Phys. Rev. E* **2012**, *86*, 031803.
- [10] M. Fritsche, D. W. Heermann, *Soft Matter* **2011**, *7*, 6906.
- [11] J. Shin, A. G. Cherstvy, R. Metzler, *New J. Phys.* **2014**, *16*, 053047.
- [12] J. M. Polson, D. R. M. Kerry, *Soft Matter* **2018**, *14*, 6360.
- [13] W. Reisner, J. N. Pedersen, R. H. Austin, *Rep. Prog. Phys.* **2012**, *75*, 106601.
- [14] T. Odijk, *Macromolecules* **1983**, *16*, 1340.
- [15] P.-G. de Gennes, "*Scaling Concepts in Polymer Physics*", Cornell University edition, Ithaca, NY, 1979.
- [16] A. Muralidhar, D. R. Tree, K. D. Dorfman, *Macromolecules* **2014**, *47*, 8446.
- [17] E. Werner, G. K. Cheong, D. Gupta, K. D. Dorfman, B. Mehlig, *Phys. Rev. Lett.* **2017**, *119*, 268102.
- [18] M. Alizadehheidaru, E. Werner, C. Noble, M. Reiter-Schad, L. K. Nyberg, J. Fritzsche, B. Mehlig, J. O. Tegenfeldt, T. Ambjörnsson, F. Persson, F. Westerlund, *Macromolecules* **2015**, *48*, 871–878.
- [19] J. Krog, M. Alizadehheidari, E. Werner, S. K. Bikkarolla, J. O. Tegenfeldt, B. Mehlig, M. A. Lomholt, F. Westerlund, T. Ambjörnsson, *The Journal of Chemical Physics* **2018**, *149*, 215101.
- [20] T. Bleha, P. Cifra, *Soft Matter* **2018**.
- [21] T. Bleha, P. Cifra, *The Journal of Physical Chemistry B* **2020**, *124*, 1691.
- [22] Y.-L. Chen, P.-k. Lin, C.-F. Chou, *Macromolecules* **2010**, *43*, 10204.
- [23] H. W. de Haan, T. N. Shendruk, *ACS Macro Letters* **2015**, *4*, 632.
- [24] J.-W. Yeh, K. Szeto, *ACS Macro Letters* **2016**, *5*, 1114.
- [25] A. Khorshid, P. Zimny, D. Tétreault-La Roche, G. Massarelli, T. Sakaue, W. Reisner, *Phys. Rev. Lett.* **2014**, *113*, 268104.
- [26] J. Zhou, Y. Wang, L. D. Menard, S. Panyukov, M. Rubinstein, J. M. Ramsey, *Nature Communications* **2017**, *8*, 807.
- [27] S. Amin, A. Khorshid, L. Zeng, P. Zimny, W. Reisner, *Nature Communications* **2018**, *9*, 1506.
- [28] S. Jun, D. Thirumalai, B.-Y. Ha, *Phys. Rev. Lett.* **2008**, *101*, 138101.
- [29] M. C. F. Pereira, C. A. Brackley, J. S. Lintuvuori, D. Marenduzzo, E. Orlandini, *The Journal of Chemical Physics* **2017**, *147*, 044908.
- [30] S. Bernier, A. Huang, W. Reisner, A. Bhattacharya, *Macromolecules* **2018**, *51*, 4012.
- [31] D. Michieletto, E. Orlandini, M. S. Turner, C. Micheletti, *ACS Macro Letters* **2020**, *9*, 1081.

- [32] Y. Jung, B.-Y. Ha, *Scientific Reports* **2019**, *9*, 869.
- [33] T. Bleha, P. Cifra, *The Journal of Chemical Physics* **2019**, *151*, 014901.
- [34] P. Cifra, T. Bleha, *Eur. Phys. J. E* **2010**, *32*, 273.
- [35] P. Cifra, T. Bleha, *Soft Matter* **2012**, *8*, 9022.
- [36] Z. Benková, P. Námer, P. Cifra, *Soft Matter* **2015**, *11*, 2279.
- [37] W. Lim, S. Y. Ng, C. Lee, Y. P. Feng, J. R. C. v. d. Maarel, *The Journal of Chemical Physics* **2008**, *129*, 165102.
- [38] C. Ji, L. Zhang, P. Wang, *Journal of Nanomaterials* **2015**, *2015*, 546851.
- [39] F. Drube, K. Alim, G. Witz, G. Dietler, E. Frey, *Nano Lett.* **2010**, *10*, 1445.
- [40] P. Cifra, Z. Benková, T. Bleha, *Phys. Chem. Chem. Phys.* **2010**, *12*, 8934.
- [41] T. Bleha, P. Cifra, *The Journal of Chemical Physics* **2018**, *149*, 054903.
- [42] J. Jia, K. Li, A. Hofmann, D. W. Heermann, *Macromol. Theory Simul.* **2019**, *28*, 1970005.
- [43] K. Ostermeir, K. Alim, E. Frey, *Phys. Rev. E* **2010**, *81*, 061802.
- [44] P. Palenčár, T. Bleha, *The Journal of Chemical Physics* **2014**, *141*, 174901.
- [45] T. W. Burkhardt, Y. Yang, G. Gompper, *Phys. Rev. E* **2010**, *82*, 041801.
- [46] J. Smrek, K. Kremer, A. Rosa, *ACS Macro Letters* **2019**, *8*, 155.
- [47] L. R. Gómez, N. A. García, T. Pöschel, *Proceedings of the National Academy of Sciences* **2020**, *117*, 3382.
- [48] G. Witz, K. Rechendorff, J. Adamcik, G. Dietler, *Phys. Rev. Lett.* **2011**, *106*, 248301.
- [49] C. Micheletti, E. Orlandini, *Soft Matter* **2012**, *8*, 10959.
- [50] R. M. Neumann, *Biophys. J.* **2003**, *85*, 3418.
- [51] A. V. Alexeev, D. V. Maltseva, V. A. Ivanov, L. I. Klushin, A. M. Skvortsov, *The Journal of Chemical Physics* **2015**, *142*, 164905.
- [52] A. Y. Grosberg, A. R. Khokhlov, "*Statistical Physics of Macromolecules*", American Institute of Physics edition, New York, 1st edn., 1994.
- [53] L. Zhu, X. Wang, J. Li, Y. Wang, *Macromol. Theory Simul.* **2016**, *25*, 482.
- [54] J. Sheng, K. Luo, *RSC Advances* **2015**, *5*, 2056.
- [55] P. Poier, C. N. Likos, R. Matthews, *Macromolecules* **2014**, *47*, 3394.